Universiteit
Leiden
The Netherlands

Giant unilamellar vesicles : an efficient membrane biophysical tool and its application in drug delivery studies

Lopez Mora, N.F.

Citation
Lopez Mora, N. F. (2016, July 7). *Giant unilamellar vesicles : an efficient membrane biophysical tool and its application in drug delivery studies*. Retrieved from https://hdl.handle.net/1887/41514

Version:	Not Applicable (or Unknown)
License:	Licence agreement concerning inclusion of doctoral thesis in the Institutional Repository of the University of Leiden
Downloaded from:	https://hdl.handle.net/1887/41514

Note: To cite this publication please use the final published version (if applicable).

Cover Page

Universiteit Leiden

The handle http://hdl.handle.net/1887/41514 holds various files of this Leiden University dissertation

Author: Lopez Mora, Nestor Fabian
Title: Giant unilamellar vesicles : an efficient membrane biophysical tool and its application in drug delivery studies
Issue Date: 2016-07-07

Chapter V

Visualisation and quantification of transmembrane ion transport into giant unilamellar vesicles

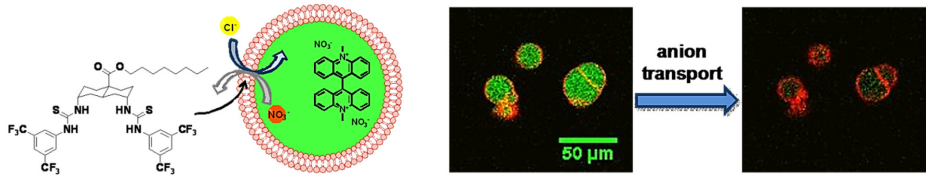

This work is published: Néstor López Mora, Hennie Valkenier, Alexander Kros, and Anthony P. Davis, *Angew. Chem., Int. Ed.,* **2015***, 54,* 2137–2141.

Abstract.

Transmembrane ion transporters (ionophores) are widely investigated as supramolecular agents with potential for biological activity. Tests are usually performed in synthetic membranes, assembled into large unilamellar vesicles (LUVs). However transport must be followed through bulk properties of the vesicle suspension, because LUVs are too small for individual study. Herein we describe an alternative approach whereby ion transport can be revealed and quantified through direct observation. The method employs giant unilamellar vesicles (GUVs), which are 20-60 μm in diameter and readily imaged by light microscopy. This allows characterisation of individual GUVs containing transporter molecules, followed by studies of transport through fluorescence emission from encapsulated indicators. The method provides new levels of certainty and relevance, given that the GUVs are similar in size to living cells. It has been demonstrated using a highly active anion carrier, and should aid the development of compounds for treating channelopathies such as cystic fibrosis.

Introduction

Transmembrane ion transport is a key process in biology. While membranes are intrinsically impermeable to ions, the cell needs to ingest and excrete charged species to sustain metabolism, avoid osmolysis and perform specialist functions. Biological ion transport is mediated by proteins,[1] but it has long been known that small molecules can have similar effects. The naturally-derived ionophore antibiotics act by promoting cation transport across cell membranes,[2] and synthetic analogues can also be effective. More recently it has been shown that anion transport is also achievable by synthetic systems,[3-5] both channels[6-8] and carriers.[9-12] In this case there is particular interest in replacing the activity of defective natural systems, yielding potential therapies for "channelopathies" such as cystic fibrosis (CF). Research on both cation and anion transport is ongoing, attracting a substantial community of bioorganic and supramolecular chemists.[13]

The study of ion transport by small molecules is commonly performed using large unilamellar vesicles (LUVs),[14] spherical assemblies of lipids ~100-200 nm in diameter in which the membrane isolates a small volume of interior aqueous solution. Transport into or out of the vesicles can then be studied by techniques such as fluorescence (using ion-sensitive fluorophores), NMR (using shift reagents to distinguish between interior and exterior), or ion selective electrodes. These methods are easy to implement but have certain disadvantages, especially for quantitative transport studies. Many of the problems relate to their small size, which is less than the wavelength of visible light and hampers imaging by light microscopy.[15] For example, while the standard method of production (extrusion through a microporous filter) allows control over size, a range of diameters are always present in a given sample. Secondly, even though unilamellar vesicles are thermodynamically favoured, the self-assembly of lipids can also produce multilamellar vesicles or other structures. Their presence may be inferred from the bulk behaviour of the suspension, but cannot be observed directly. Thirdly, a typical experiment on the LUV suspension will involve addition of a transporter or substrate, then the observation of a change (e.g. in bulk fluorescence) which reports transport into or out of vesicles. In principle the same change can often be produced by vesicle bursting rather than transport. While circumstances and controls may suggest that bursting is unlikely, doubts may persist. Fourthly, the LUVs are about two orders of magnitude smaller than most cells, which affects their value as cell models. In particular, the LUVs possess much higher surface:volume

ratios which increases their sensitivity to transport processes (see discussion below). Agents that cause major changes in LUVs may thus have limited potential for biological activity.

Herein we report a new method for studying ion transport which circumvents the above problems and allows direct, unambiguous observation of the transport process. Instead of LUVs, the method employs individual giant unilamellar vesicles (GUVs)[16] with diameters of 20-60 µm, similar to many cells and readily observable by microscopy. Fluorescence microscopy of GUVs has been used to study passive diffusion of peptides[17] and organic compounds[18] through membranes, passive diffusion of dyes through pores formed by peptides[19-22] or proteins[23, 24] and to qualitatively study the presence and performance of membrane proteins.[25] However, as far as we know, this is the first report in which the technique has been applied to the transport of inorganic ions. The method has been used to visualise and quantify chloride transport by a powerful anion transporter, and could in principle be applied to many other ion transport processes.

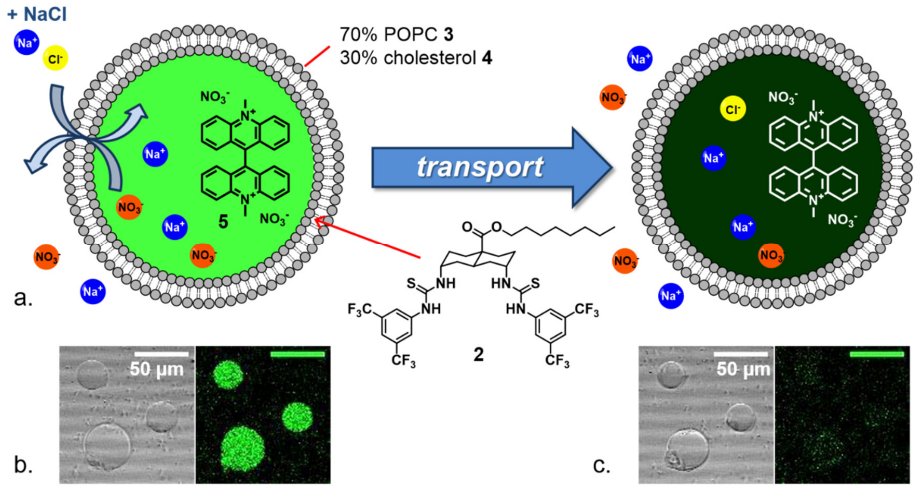

Figure 1. a) Schematic of the transport of chloride by transporter **1** into giant unilamellar vesicles (GUVs). Upon addition of a solution of NaCl, the transporter exchanges exterior chloride for interior nitrate. The chloride that is transported into the GUVs quenches the fluorescence of lucigenin **2** present in the interior of the vesicles. **b,c**) Bright field (left) and confocal fluorescence microscopy images (right) show three giant vesicles with transporter **1** (0.1 mol% of total lipid) preincorporated in the membrane before (b) and after (c) addition of NaCl.

The new method as applied herein is illustrated in **Figure 1**. The transport process is Cl^-/NO_3^- exchange by the bis-(thioureido)decalin **1**, an anion carrier (anionophore) which has recently been prepared by the Bristol group.[26] Giant vesicles are formed in which the transporter is located in the bilayer membrane and the chloride-sensitive fluorophore lucigenin **2** is trapped in the aqueous interior. Both interior and exterior aqueous phases contain $NaNO_3$ (225 mM). When NaCl is added to the exterior solution, the chloride is carried through the membrane by **1** and makes contact with lucigenin, quenching fluorescence.[27-31] Counter-transport of nitrate maintains electroneutrality.

The transfer of this assay to GUVs required a powerful transporter. Absolute transport rates into vesicles depend on the surface area, while the rate of change of substrate concentration depends on the interior volume. For a given vesicle composition, d[substrate]/dt scales with the surface:volume ratio, which decreases linearly with vesicle diameter (see *Experimental Section*). Concentration changes for a 20 μm GUV should therefore be 100 times slower than for a 200 nm LUV, and only the more active transporters are likely to give observable effects. Anionophore **1** features strongly anion-binding thioureido groups preorganised on a trans-decalin scaffold,[32] and a uniformly lipophilic exterior which appears to favour passage through bilayer membranes. It had shown exceptional activity in conventional LUV-based transport experiments[26] and was therefore most likely to succeed in the new test system.

Also needed was a method for preparing GUVs of well-defined size from lipids doped with transporter, at high ionic strength and with a cholesterol rich lipid mixture. The problem was solved using a technique developed by the Leiden group, in which the GUVs are grown on a cross-linked dextran-(polyethylene glycol) hydrogel substrate.[33] Adjusting the density of cross-links allows control of vesicle size between ~20 and ~100 μm. In the present case GUVs were grown from 1-palmitoyl-2-oleoylphosphatidylcholine (POPC) and cholesterol (7:3 ratio), plus a varied amount of transporter **1** (0 mol%, 0.01 mol%, 0.04 mol%, and 0.1 mol% of total lipid), using a hydrogel designed to yield vesicles of 10-40 μm diameter (see *Experimental Section*). The hydrogel with the lipid film containing the transporter was rehydrated with a solution of 225 mM $NaNO_3$, 0.8 mM lucigenin and 200 mM sucrose. The resulting giant vesicles were transferred into a microscopy chamber and the external solution was replaced by perfusion with a solution of 225 mM $NaNO_3$ and 200 mM glucose. This procedure removed the external lucigenin while lowering the density of the medium, causing the GUVs to settle on the viewing surface. The giant vesicles were imaged both in bright-field mode and when

excited with a 488 nm laser in a confocal fluorescence microscope. After 30-60 seconds, 25 µL 1 M NaCl solution was added to the microscopy chamber with a microsyringe, giving rise to an external chloride concentration of ~50 mM. As expected, the intensity of lucigenin emission was observed to decay significantly over a period of ~5 minutes (**Figure 2**). Bright-field images confirmed the presence of intact GUVs after quenching (see **Figure 1b,c** and *Experimental Section*), showing that the apparent disappearance of vesicles was not due to bursting. No fluorescence decay was observed in the absence of transporter (**Figures 2a,e**), and the rate of decay was clearly dependent on the amount of transporter **1** added (**Figures 2b-d, f-h**). The possibility of dye leakage was ruled out by a control experiment in which lucigenin was replaced by carboxyfluorescein. In this case, fluorescence emission from the vesicles underwent negligible change (see **Figure** 7 in *Experimental Section*). Our studies thus provide unambiguous confirmation that bis-thiourea **1** does indeed promote chloride transport across bilayer membranes, while preserving the lipid membrane and GUV integrity.

To obtain more insight into the process, we quantified the fluorescence intensity of the giant vesicles within each frame of the recorded time lapses. We then normalised and averaged the fluorescence intensities of the vesicles within one chamber (and from one NaCl addition experiment) to obtain curves that show the average fluorescence over time (**Figure 3**).

The experiment was performed twice for most concentrations and four times with the GUVs containing 0.01% transporter. **Figure 3** clearly shows how quenching and thus anion transport is fastest when 0.1% transporter is present (red) and how it is only slightly slower when 0.04% transporter is present (blue). When only 0.01% transporter is present (green), the fluorescence intensity has not yet plateaued within 250 seconds and transport is still ongoing. For this reason, the fluorescence intensities of the GUVs with 0.01% transporter were monitored over 20 minutes (see **Figures A1-A11** in *Annex Chapter V* for the full data sets). We also monitored the fluorescence intensity of GUVs over time without adding NaCl to test for photobleaching of lucigenin. As indicated by the black line in **Figure 3** in *Experimental Section* and **Figure A11** in *Annex Chapter V*), no photobleaching was observed in the first 5 minutes and even after 20 minutes of monitoring the bleaching was still below 7%, which is insignificant compared to the loss of fluorescence by quenching caused by transport of chloride.

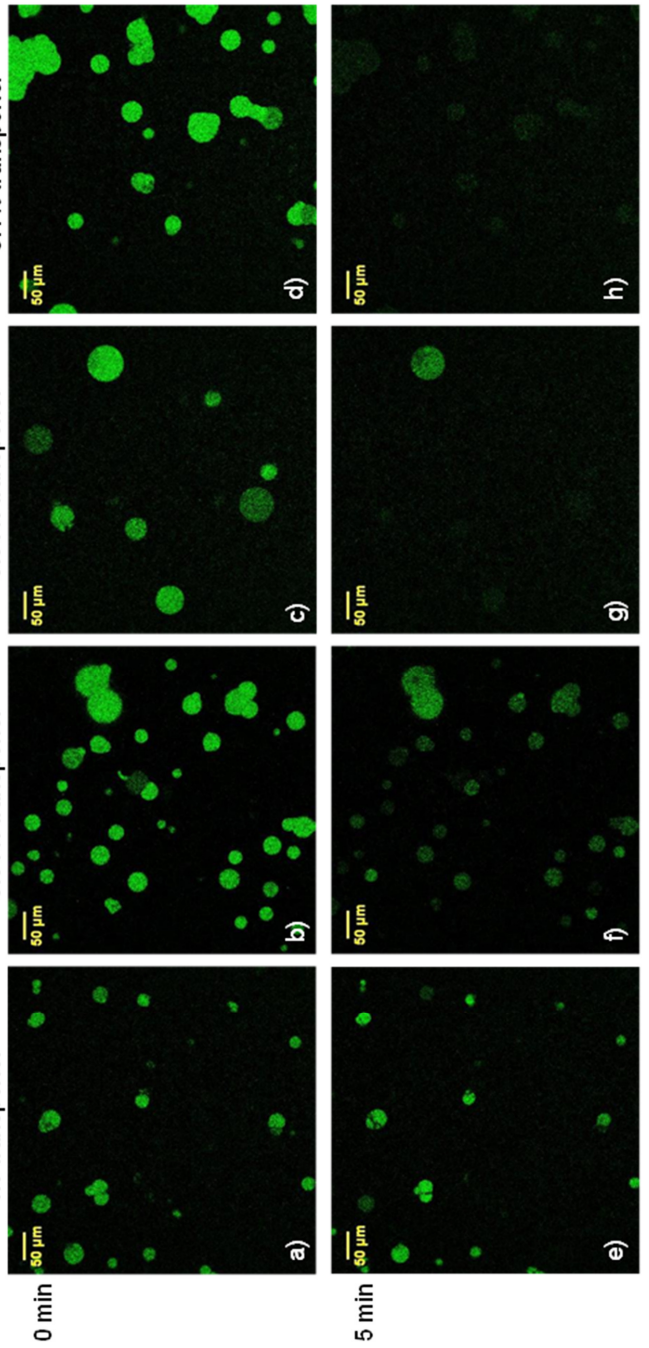

Figure 2. Confocal fluorescence microscopy images of lucigenin-containing GUVs, incorporating varying amounts of transporter **1**, before (a-d) and after addition of NaCl (e-f: images taken ~5 min after the addition of NaCl).

Careful examination of all the fluorescence decay profiles reveals that while most GUVs within one experiment have similarly shaped fluorescence *vs.* time curves (forming a distribution due to the variation in sizes of the vesicles), certain vesicles show distinct behaviour (see full datasets in the *Annex Chapter V*). For instance, the fluorescence of one giant vesicle in **Figure 2g** remains visible where all the others have disappeared into the background (these distinctively slower traces have not been included in the average curves in **Figure 3**). Suspecting that this distinct transport behaviour was due to multilamellarity of certain vesicles, we repeated the experiments employing 0.01% and 0.04% transporter with lissamine rhodamine B-labelled lipid added to the membrane (0.1 mol%) (see **Figure A12** in *Annex Chapter V*). This allowed us to visualise the membranes of the vesicles upon excitation with a 532 nm laser. Multilamellar membranes give higher intensities of rhodamine fluorescence compared to unilamellar membranes.[34] The results of one of these experiments employing 0.01% transporter **1** are presented in **Figure 4**. For typical GUVs the intensity of red fluorescence emitted from the membranes is ~25 units. However, for the vesicles labelled C and D in **Figure 4a** the observed intensity is double this value (~50 units) while the intensities from the membranes of GUVs A and B reach 200-250 and 100-150 units respectively (for details see **Fig. A12**, full datasets in *Annex Chapter V*). In **Figure 4b** we clearly see that the vesicles labelled A-D display a stronger intensity of fluorescence of lucigenin, even after 20 minutes. This is also seen in the normalized fluorescence traces of the individual vesicles as plotted in **Figure 4c**. After 1000 seconds the fluorescence intensity of most vesicles has reached the plateau value of ~20% of the initial fluorescence, while plots from vesicles A-D show much slower decays. As giant vesicles C and D show a rhodamine emission intensity which is double the value of the majority of the vesicles, and both have identical curves, these are likely to have a double lipid bilayer. Vesicles A and B, with even stronger rhodamine emission and slower lucigenin quenching, are likely to have higher orders of multilamellarity. Vesicles A-D are therefore excluded from further quantitative analysis.

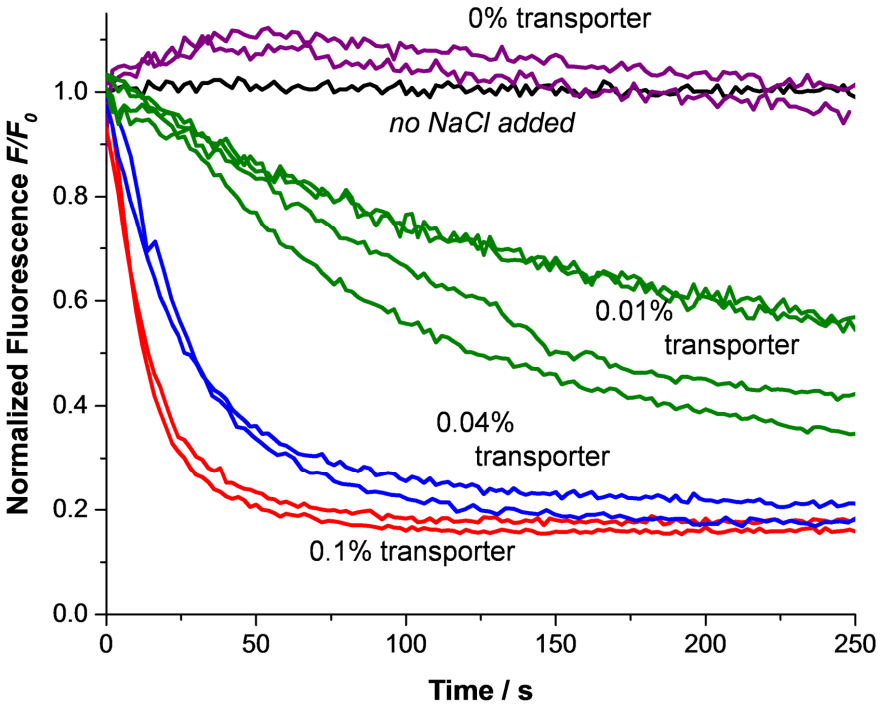

Figure 3. Average traces of the normalised lucigenin emission intensity after addition of 50 mM NaCl to GUVs without transporter (purple), with 0.01% transporter (green), with 0.04% transporter (blue) and with 0.1% transporter present (red) or without NaCl added (black).

Having found a method to distinguish unilamellar and multilamellar giant vesicles, we were able to quantify transport into the unilamellar vesicles. We focused on the slower-transporting GUVs containing 0.01% bis-thiourea **1**, to minimise errors due to the addition of NaCl at the start of the experiment. Relatively slow and careful addition is necessary to avoid disturbing the GUVs in the field of the microscope. The fluorescence decay data were analysed using a protocol previously employed for **1** in LUVs.[26] Values for F_0/F [35] were fitted to a single exponential decay function, which was converted to chloride concentrations by assuming a limiting intravesicular [Cl^-] of 50 mM. This was then used to calculate an initial rate of chloride transport per transporter molecule, taking account of the size of the vesicle. The analysis was performed for 56 GUVs from 6 experiments (all with 0.01% transporter), giving an average initial rate per transporter of 820 ± 260 Cl^- s^{-1}. This value is similar to that obtained from experiments on bulk LUV solutions using the same transporter (850 Cl^- s^{-1}).[26] However,

because the present work was performed on vesicles of known diameters and lamellarities, characterised by microscopy, we believe it is much more reliable. For a full description of the analysis procedure, see the *Experimental Section*.

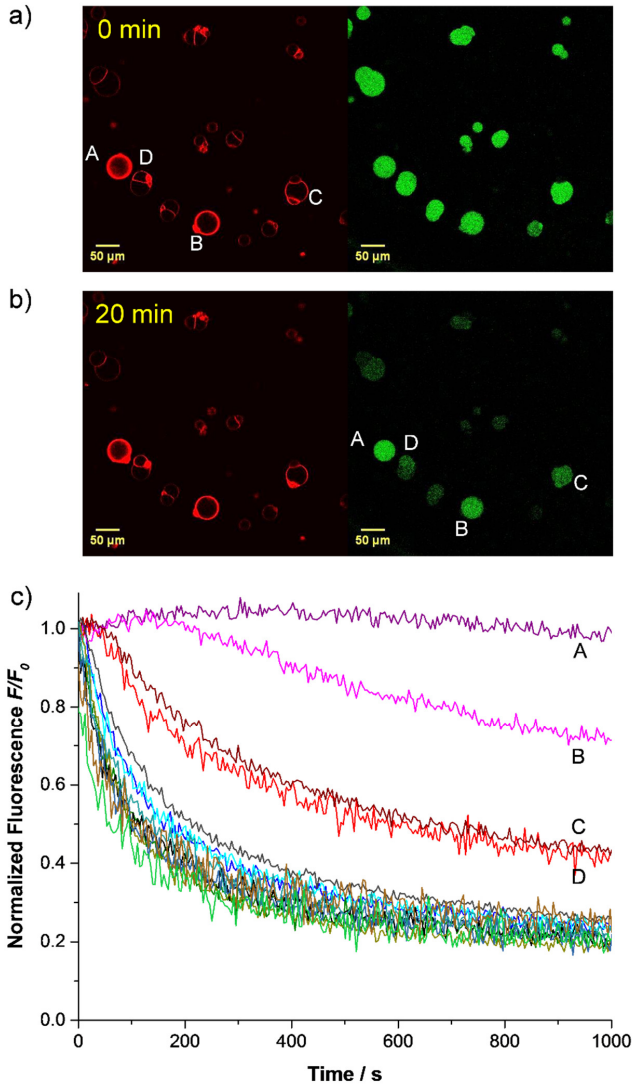

Figure 4. a) Fluorescence microscopy images of GUVs containing lucigenin and incorporating rhodamine-labelled lipid + 0.01% transporter **1**. Left: Illumination at 532 nm visualises the rhodamine in the bilayer. Right: Illumination at 488 nm excites the lucigenin. **b**) As above, 20 min after addition of NaCl. **c**) Traces of the lucigenin fluorescence intensity of individual vesicles over time after addition of 50 mM NaCl. The four vesicles that display stronger rhodamine fluorescence, and their corresponding traces, are labelled A-D.

Conclusion

In conclusion we have devised a new method whereby ion transport by small molecules into individual giant unilamellar vesicles can be observed and quantified. By directly visualising transport into GUVs, the approach offers a high level of certainty and integrity compared to experiments on bulk suspensions of smaller vesicles. Instead of quantifying transport into a population of vesicles with a distribution of sizes, we can now analyse the transport into individual GUVs of which we can verify the lamellarity and measure the size. The method is complementary to studies in LUVs, in that it is better suited to very powerful transporters which can produce measurable effects despite the low surface:volume ratio of GUVs. Indeed, positive results in this test provide clear encouragement that a transporter has potential for biological activity.

In this initial demonstration the method has been used to study chloride/nitrate exchange by an anion carrier. However, it is reasonable to suppose that other types of ion transport could be investigated similarly. A number of fluorescence-based methods have been developed for following transport into LUVs.[14] For example, the pH-sensitive probe 8-hydroxy-1,3,6-pyrenetrisulfonate (HPTS) is used as a general indicator of ion transport, while other dyes have been used to follow transport of specific metal cations. Transfer of these assays to GUVs should be straightforward, while further indicators are readily available[36] and remain to be exploited.

Finally, the success of **1** at mediating Cl^-/NO_3^- exchange in this system, even at the modest loading of 0.01%, further highlights its exceptional activity. This molecule is relatively lipophilic so that dispersion in water and delivery to cell membranes may be challenging. However if the delivery problem can be solved, for example with membrane fusion,[37, 38] the effectiveness of **1** in cell-sized vesicles augurs well for applications in biology and medicine.

Experimental Section

Materials and methods

Cholesterol, 1-palmitoyl-2-oleoyl-sn-glycero-3-phosphocholine (POPC), and bovine serum albumin (BSA) were purchased from Sigma Aldrich. 1,2-Dioleoyl-sn-glycero-3-phosphoethanolamine-N-(lissamine rhodamine B sulfonyl) (ammonium salt) (rhodamine labelled lipid) was purchased from Avanti Polar Lipids and 10,10'-dimethyl-9,9'-biacridinium nitrate (lucigenin, 2) was purchased from Tokyo Chemical Industry UK Ltd. Chloroform was deacidified by passage through a column containing activated basic alumina before the preparation of the lipid solutions. The lucigenin (0.8 mM), $NaNO_3$ (225 mM) and NaCl (1 M) aqueous solutions were prepared with Millipore grade water. Lipid solutions of POPC and cholesterol (70:30 ratio, 14 mM) were prepared in the previously deacidified chloroform and the transporter octyl t-(2,7)-bis(3-(3,5-bis(trifluoromethyl)phenyl)thioureido)-t-8a-decahydronaphthalene-r-4a-carboxylate,[26] (1, 84 μM solution in methanol) was added to this lipid solution at 0.01 mol%, 0.04 mol% and 0.1 mol% (relative to total lipid). Rhodamine labelled lipid was added in 0.1 mol% when membrane imaging was required.

GUVs formation and microscopy chamber preparation

Giant Unilamellar Vesicles (GUVs) were grown in Dex-PEG (1:1 ratio) coated microscope glass slides substrates as described previously.[33] Lipid solution (10 μL) was deposited on a hydrogel coated glass slide, then the lipid solution was dried by evaporating the chloroform under a gentle stream of Nitrogen gas. A liquid chamber was made by placing a 15 mm (OD) glass O-Ring on top of the hydrogel and sealed with high vacuum silicon grease. The lipid film was rehydrated by adding 400 μL of an aqueous solution that contains lucigenin (0.8 mM), $NaNO_3$ (225 mM) and sucrose (200 mM), into each chamber. GUVs were grown during at least 3 hours at room temperature and subsequently the solution with free floating GUVs was transferred into an eppendorf tube containing 600 μL of $NaNO_3$ (225 mM) and glucose (200 mM) aqueous solution. The visualization chamber (μ-Slide 8 well, Ibidi) was pre-treated with an aqueous solution of BSA (1 mg/mL, 500 μL) for one hour. The diluted solution with GUVs was transferred into the microscopy visualization chamber (500 μL per well). The GUVs were left to sediment for at least 30 minutes and the excess of non-encapsulated lucigenin was replaced by the $NaNO_3$ and glucose solution using a peristaltic perfusion pump (Instech P720,

~ 0.4 mL/min, 30 minutes), to produce a clean background for imaging the encapsulated lucigenin dye in the GUVs.

Lucigenin quenching assay

During the imaging of the GUVs in a time lapse experiment, 25 µL 1M NaCl (in NaNO3 and glucose solution) was added to the well after 30-60 seconds with a microsyringe, giving a final NaCl concentration of ~50 mM.

Fluorescence Microscopy of GUVs

All imaging was performed on a Leica TCS SPE confocal microscope system. Illumination was provided by a solid state laser using the 488 nm laser line (15% laser power) for scanning lucigenin's fluorescence and 532 nm laser line (10-15% laser power) for scanning lissamine rhodamine's fluorescence. Confocal microscopy was carried out using a 20× dry objective. The analysis of the images was performed in ImageJ software, by measuring the average intensity of an area corresponding to one GUV for the series of time lapsed confocal image frames.

Osmomolality

The osmolality of a NaNO3 (225 mM) solution was determined from the freezing point depression using an Osmometer Roebling Type 13 (calibrated using 100 mOsm/kg NaCl standard solution) and found to be 378 mOsm/kg (standard PBS buffer was 310 mOsm/kg). Addition of 50 mM NaCl to 225 mM NaNO3 causes the osmolality to increase to 473 mOsm/kg.

Fitting of the fluorescence intensities of individual GUVs

According to the Stern-Volmer relationship:

$$\frac{F_0}{F} = 1 + k_q \tau_0 \, [Q]$$

the fluorescence in absence of quencher (F_0) divided by the fluorescence (F) is proportional to the concentration of quencher [Q], which is chloride in our experiments. In the Stern-Volmer equation k_q is the rate constant of the quenching process and τ_0 is the life time of the emitting state of lucigenin, which are both constants. This allows us to take the reciprocal of our

normalized fluorescence traces (which are F/F_0) to get F_0/F curves, of which the shape directly represents the concentration of chloride in the vesicles over time.

The first 1000 s of the F_0/F curves obtained for individual GUVs (0.01% transporter) are fitted with a single exponential decay function:

$$\frac{F_0}{F} = y - a \cdot e^{-kt} \quad (1)$$

Examples of representative fits are given in **Figure 5**.

We note that the increase of the noise in the curves presented in **Figure 5** is caused by the decrease of fluorescence intensity upon quenching. The error in measuring the fluorescence intensity thus increases over time when transport is occurring.

The value obtained for parameter k is the rate constant for the transmembrane transport process. Since the fits are generally good we can assume that the concentration of chloride inside the GUV [Cl^-] increases from 0 to 50 mM following the exponential decay function given by equation 2:

$$[Cl^-] = 50\ mM(1 - e^{-kt}) \quad (2)$$

The rate constant k is obtained from the fit. Differentiation of equation 2 at t=0 gives the initial rate of chloride transport into the GUVs as 50k in mM s^{-1}. From the measured diameter of the GUVs, the volume and the surface area can be calculated. Subsequently, the initial rate (in mM s^{-1}) can be multiplied by the volume of the GUV (V_{GUV}) and Avogadro's number (N_A) to get the initial rate as number of chloride anions transported into the GUV per second. Dividing this by the calculated number of transporters in the GUVs (two times the surface area A_{GUV}, divided by the surface area per lipid which is assumed to be 46.97 $Å^2$ for POPC/cholesterol 7:3[26, 39] times the ratio of transporter to lipid) gives the initial rate of transport per transporter ($I_{transporter}$) in chloride anions per second (equation 3).

$$I_{transporter} = \frac{50\ mM \cdot k \cdot V_{GUV} \cdot N_A}{\left(\frac{2 \cdot A_{GUV}}{46.97\ Å^2}\right)\left(\frac{transporter}{lipid}\right)} \quad (3)$$

Data on 56 GUVs from 6 experiments were analyzed this way, giving an average initial rate per transporter of 820 ± 260 $Cl^-\ s^{-1}$.

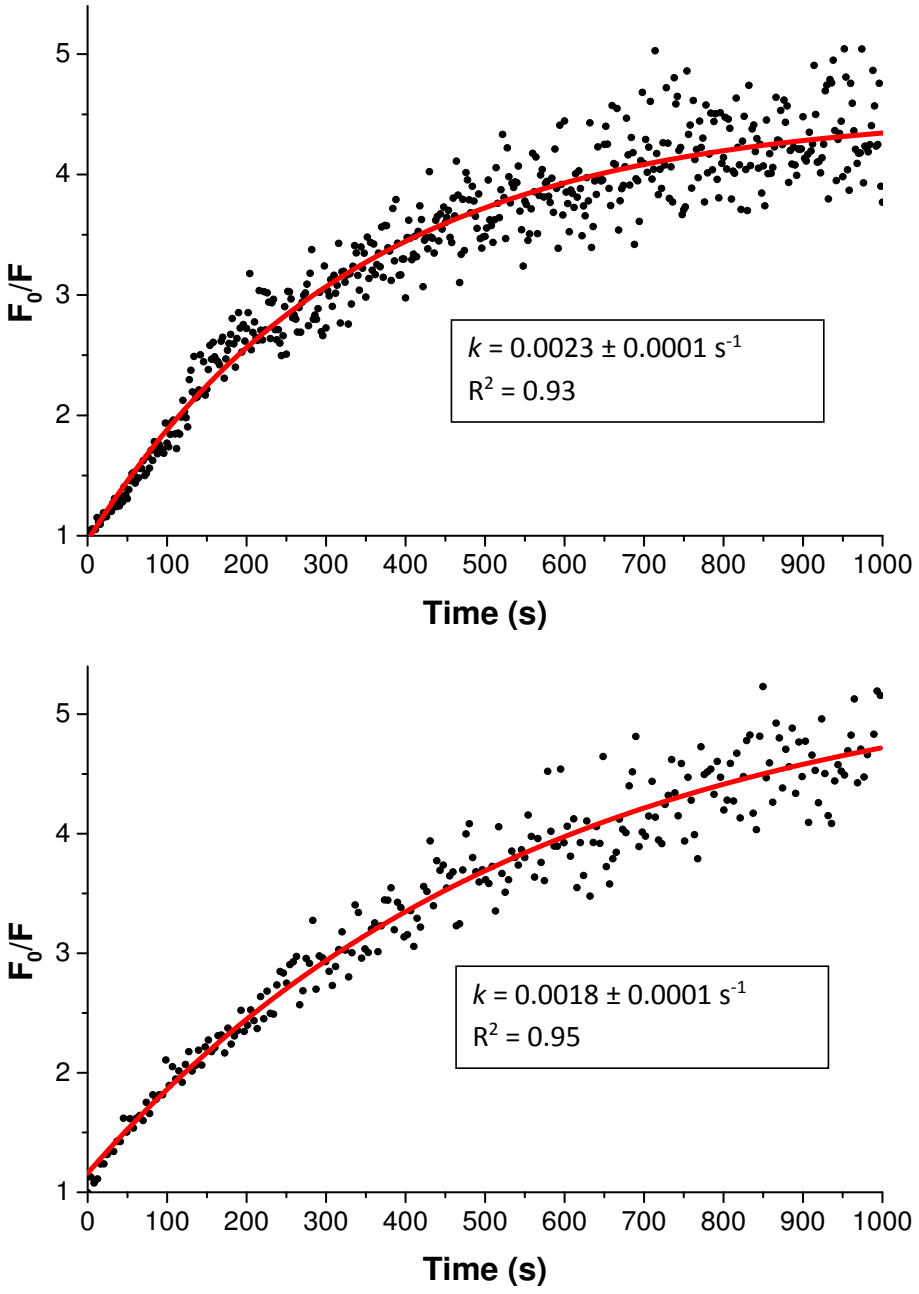

Figure 5. Single exponential fits (red lines) of F_0/F data of individual GUVs (black dots). Note that the noise level of the measured data increases over time. Due to the decreasing fluorescence intensity, the error in measuring the average fluorescence intensity of the area corresponding to a GUV increases.

The half-life of the transport process increases linearly with the diameter of the GUVs

The rate of transport by one transporter molecule is independent of the size of the GUV. However, the first-order rate constant for the transport of chloride into the GUVs (k), as obtained from the fits, depends on the volume of the GUV (V_{GUV}) and on the number of transporters present in the membrane and thus on the surface area (A_{GUV}), according to equation (3). From this it can be shown as follows that, for a given transporter at a given concentration, the half-life ($t_{½}$) is directly proportional to the diameter of the GUVs:

As $I_{transporter}$ is a constant, $\frac{k \cdot V_{GUV}}{A_{GUV}}$ must also be constant, indicating that $k \propto \frac{A_{GUV}}{V_{GUV}}$

For half-life ($t_{½}$) one can therefore write:

$t_{½} = \frac{\ln(2)}{k} \propto \frac{V_{GUV}}{A_{GUV}} \propto \emptyset_{GUV}$ (where $\emptyset_{GUV}$ is the diameter of the GUVs)

Figure 6a gives a plot of the half-lives obtained for the 16 GUVs from one experiment, which show a nearly linear relationship with diameter of the GUVs. The plot in **Figure 6b** shows the half-lives from all the GUVs of six experiments (all with 0.01% transporter). The latter plot shows more deviations from the linear relationship between the half-life and the diameter, but the main trend is still linear, indicating how the size of the GUVs affects the observed rate of quenching of the fluorescence.

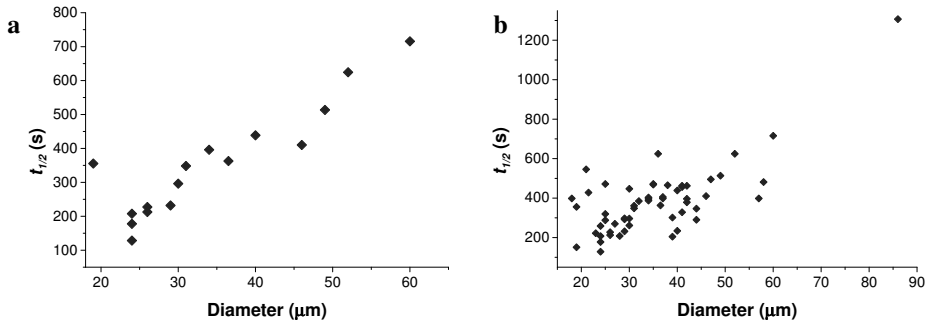

Figure 6. Plot of the half-lives (from single exponential fits, experiments with 0.01% transporter) versus the diameter of 16 individual GUVs from one experiment (**a**) and from 56 GUVs of 6 experiments combined in one graph (**b**).

Test for leaking of a fluorescence dye from the GUVs

To exclude the possibility that the decrease of fluorescence of the GUVs is caused by lucigenin leaking out the GUVs via defects formed by the transport and chloride, we repeated the experiment with carboxyfluorescein as the fluorescent dye.[40] As the fluorescence of carboxyfluorescein is not quenched by chloride, we should be able to distinguish between the dye leaking from the GUVs and transport of chloride into the GUVs.

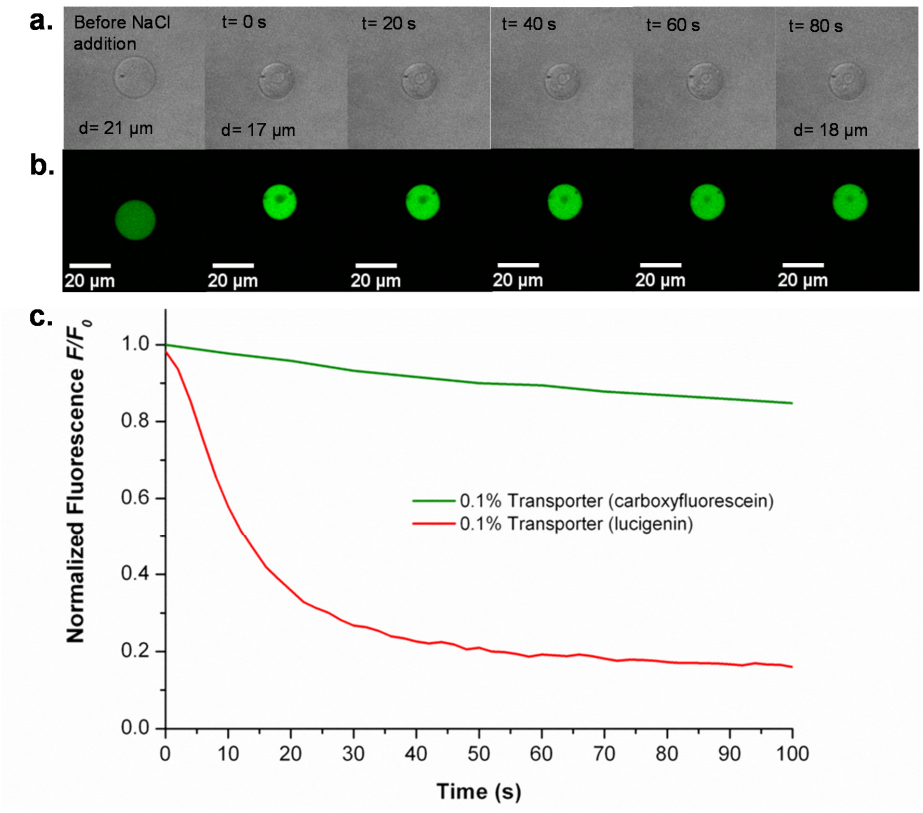

Figure 7. Series of bright-field (**a.**) and fluorescence microscopy images (**b.**) of a GUV made of POPC (70%), cholesterol (30%), and transporter **1** (0.1%) containing carboxyfluorescein (0.1 mM, pH 7) and $NaNO_3$ (225 mM, interior and exterior). The confocal fluorescence imaging is performed with a 488 nm laser at 10% power and a detection filter band between 500-600 nm. Upon the addition of NaCl (25 µL, 1 M) the GUVs shrink producing an increase in the fluorescence, which slightly decreases once the inner content and the exterior reach the equilibrium. **c.** Comparison of the experiments with carboxyfluorescein and lucigenin. The red line corresponds to the average fluorescence of lucigenin with 0.1 % transporter preincorporated in the membrane (see Figure 3 of the main paper). The green line shows the average fluorescence of carboxyfluorescein of 5 individual GUVs with

0.1 % transporter preincorporated in the membrane. The starting time (t = 0 s) corresponds to the addition of 25 µL NaCl (1M).

The results in **Figure 7** show that carboxyfluorescein does not leak from the GUVs. We can therefore conclude that the addition of sodium chloride to the GUVs with transporter does not cause the formation of defects or channels in the membrane. This confirms that the observed quenching of fluorescence of lucigenin is caused by chloride transport into the GUVs.

References

1. Hille, B. Ion Channels of Excitable Membranes. *Sinauer, Sunderland, MA* (2001).
2. Pressman, B.C. Biological Applications of Ionophores. *Annu Rev Biochem* **45**, 501-530 (1976).
3. Davis, A.P., Sheppard, D.N. & Smith, B.D. Development of synthetic membrane transporters for anions. *Chem Soc Rev* **36**, 348-357 (2007).
4. Davis, J.T., Okunola, O. & Quesada, R. Recent advances in the transmembrane transport of anions. *Chem Soc Rev* **39**, 3843-3862 (2010).
5. Busschaert, N. & Gale, P.A. Small-Molecule Lipid-Bilayer Anion Transporters for Biological Applications. *Angew Chem Int Edit* **52**, 1374-1382 (2013).
6. Mareda, J. & Matile, S. Anion-pi Slides for Transmembrane Transport. *Chem-Eur J* **15**, 28-37 (2009).
7. Gokel, G.W. & Negin, S. Synthetic Ion Channels: From Pores to Biological Applications. *Accounts Chem Res* **46**, 2824-2833 (2013).
8. Li, X., Shen, B., Yao, X.Q. & Yang, D. Synthetic Chloride Channel Regulates Cell Membrane Potentials and Voltage-Gated Calcium Channels. *J Am Chem Soc* **131**, 13676-13680 (2009).
9. Valkenier, H. & Davis, A.P. Making a Match for Valinomycin: Steroidal Scaffolds in the Design of Electroneutral, Electrogenic Anion Carriers. *Accounts Chem Res* **46**, 2898-2909 (2013).
10. Cooper, J.A., Street, S.T.G. & Davis, A.P. A Flexible Solution to Anion Transport: Powerful Anionophores Based on a Cyclohexane Scaffold. *Angew Chem Int Edit* **53**, 5609-5613 (2014).
11. Jentzsch, A.V., Hennig, A., Mareda, J. & Matile, S. Synthetic Ion Transporters that Work with Anion-pi Interactions, Halogen Bonds, and Anion-Macrodipole Interactions. *Accounts Chem Res* **46**, 2791-2800 (2013).
12. Gale, P.A., Perez-Tomas, R. & Quesada, R. Anion Transporters and Biological Systems. *Accounts Chem Res* **46**, 2801-2813 (2013).
13. Matile, S. & Fyles, T. Transport Across Membranes. *Accounts Chem Res* **46**, 2741-2742 (2013).
14. Matile, S. & Sakai, N. Analytical methods in supramolecular chemistry (Ed. C. A. Schalley). *Wiley-VCH, Weinheim*, pp. 711-742 (2012).
15. Stamou, D., Duschl, C., Delamarche, E. & Vogel, H. Self-assembled microarrays of attoliter molecular vessels. *Angew Chem Int Edit* **42**, 5580-5583 (2003).
16. Walde, P., Cosentino, K., Engel, H. & Stano, P. Giant Vesicles: Preparations and Applications. *Chembiochem* **11**, 848-865 (2010).
17. Shimanouchi, T. et al. Permeation of a beta-heptapeptide derivative across phospholipid bilayers. *Bba-Biomembranes* **1768**, 2726-2736 (2007).
18. Li, S., Hu, P.C. & Malmstadt, N. Confocal Imaging to Quantify Passive Transport across Biomimetic Lipid Membranes. *Anal Chem* **82**, 7766-7771 (2010).
19. Tamba, Y. & Yamazaki, M. Single giant unilamellar vesicle method reveals effect of antimicrobial peptide magainin 2 on membrane permeability. *Biochemistry-Us* **44**, 15823-15833 (2005).
20. Tamba, Y. & Yamazaki, M. Magainin 2-Induced Pore Formation in the Lipid Membranes Depends on Its Concentration in the Membrane Interface. *J Phys Chem B* **113**, 4846-4852 (2009).

21. Tamba, Y., Ariyama, H., Levadny, V. & Yamazaki, M. Kinetic Pathway of Antimicrobial Peptide Magainin 2-Induced Pore Formation in Lipid Membranes. *J Phys Chem B* **114**, 12018-12026 (2010).
22. Islam, M.Z., Ariyama, H., Alam, J.M. & Yamazaki, M. Entry of Cell-Penetrating Peptide Transportan 10 into a Single Vesicle by Translocating Across Lipid Membrane and Its Induced Pores. *Biochemistry-Us* **53**, 386-396 (2014).
23. Robinson, T., Kuhn, P., Eyer, K. & Dittrich, P.S. Microfluidic trapping of giant unilamellar vesicles to study transport through a membrane pore. *Biomicrofluidics* **7** (2013).
24. Alam, J.M., Kobayashi, T. & Yamazaki, M. The Single-Giant Unilamellar Vesicle Method Reveals Lysenin-Induced Pore Formation in Lipid Membranes Containing Sphingomyelin. *Biochemistry-Us* **51**, 5160-5172 (2012).
25. Dezi, M., Di Cicco, A., Bassereau, P. & Levy, D. Detergent-mediated incorporation of transmembrane proteins in giant unilamellar vesicles with controlled physiological contents. *P Natl Acad Sci USA* **110**, 7276-7281 (2013).
26. Valkenier, H. et al. Preorganized Bis-Thioureas as Powerful Anion Carriers: Chloride Transport by Single Molecules in Large Unilamellar Vesicles. *J Am Chem Soc* **136**, 12507-12512 (2014).
27. McNally, B.A., Koulov, A.V., Smith, B.D., Joos, J.B. & Davis, A.P. A fluorescent assay for chloride transport; identification of a synthetic anionophore with improved activity. *Chem Commun*, 1087-1089 (2005).
28. McNally, B.A. et al. Structure-Activity Relationships in Cholapod Anion Carriers: Enhanced Transmembrane Chloride Transport through Substituent Tuning. *Chem-Eur J* **14**, 9599-9606 (2008).
29. Busschaert, N. et al. Towards predictable transmembrane transport: QSAR analysis of anion binding and transport. *Chem Sci* **4**, 3036-3045 (2013).
30. Bahmanjah, S., Zhang, N. & Davis, J.T. Monoacylglycerols as transmembrane Cl- anion transporters. *Chem Commun* **48**, 4432-4434 (2012).
31. Dawson, R.E. et al. Experimental evidence for the functional relevance of anion-pi interactions. *Nat Chem* **2**, 533-538 (2010).
32. Hussain, S., Brotherhood, P.R., Judd, L.W. & Davis, A.P. Diaxial Diureido Decalins as Compact, Efficient, and Tunable Anion Transporters. *J Am Chem Soc* **133**, 1614-1617 (2011).
33. Mora, N.L. et al. Preparation of size tunable giant vesicles from cross-linked dextran(ethylene glycol) hydrogels. *Chem Commun* **50**, 1953-1955 (2014).
34. Chiba, M., Miyazaki, M. & Ishiwata, S. Quantitative Analysis of the Lamellarity of Giant Liposomes Prepared by the Inverted Emulsion Method. *Biophys J* **107**, 346-354 (2014).
35. Note that F0/F is the reciprocal of the quantity shown in Figures 3 and 4. The analysis employs F0/F because, according to the Stern-Vollmer equation, it is this value which is directly proportional to quencher concentration.
36. Haugland, R.P. Handbook of Fluorescent Probes and Research Chemicals. *Invitrogen (Molecular Probes), Eugene, OR* (2005).

37. Marsden, H.R., Elbers, N.A., Bomans, P.H.H., Sommerdijk, N.A.J.M. & Kros, A. A Reduced SNARE Model for Membrane Fusion. *Angew Chem Int Edit* **48**, 2330-2333 (2009).

38. Zope, H.R. et al. In Vitro and In Vivo Supramolecular Modification of Biomembranes Using a Lipidated Coiled-Coil Motif. *Angew Chem Int Edit* **52**, 14247-14251 (2013).

39. Olsen, B.N., Schlesinger, P.H. & Baker, N.A. Perturbations of Membrane Structure by Cholesterol and Cholesterol Derivatives Are Determined by Sterol Orientation. *J Am Chem Soc* **131**, 4854-4865 (2009).

40. Ambroggio, E.E., Separovic, F., Bowie, J.H., Fidelio, G.D. & Bagatolli, L.A. Direct visualization of membrane leakage induced by the antibiotic peptides: Maculatin, citropin, and aurein. *Biophys J* **89**, 1874-1881 (2005).

Annex
Chapter V

Full datasets behind the average curves presented in Figure 3 of the main paper

Cross-sections of vesicles with rhodamine-labelled membranes in Figure 4a

Full datasets behind the average curves presented in Figure 3 of the main paper

No transporter

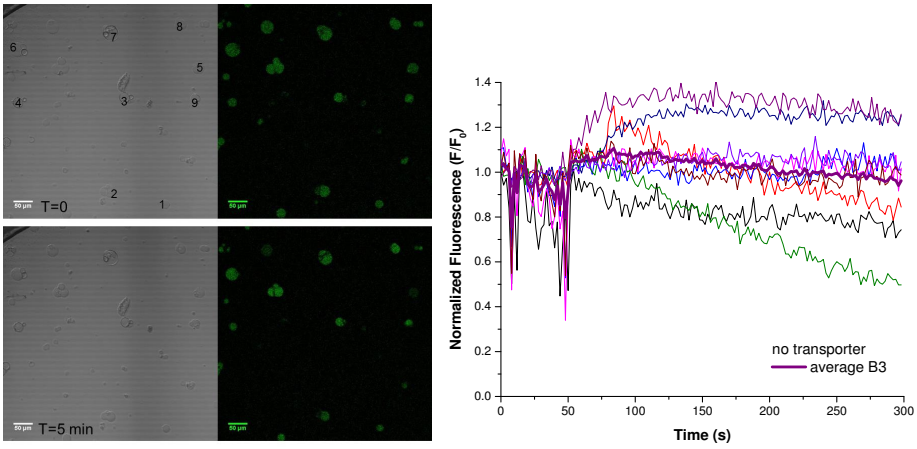

Figure A1. Bright-field and fluorescence microscopy images before (top) and after (bottom) addition of NaCl to GUVs without transporter (*experiment B3*). The normalized fluorescence intensity over time is given for the individual numbered GUVs and for the average of all numbered GUVs (fat purple line). The average diameter of the GUVs used in the average trace for 36 µm.

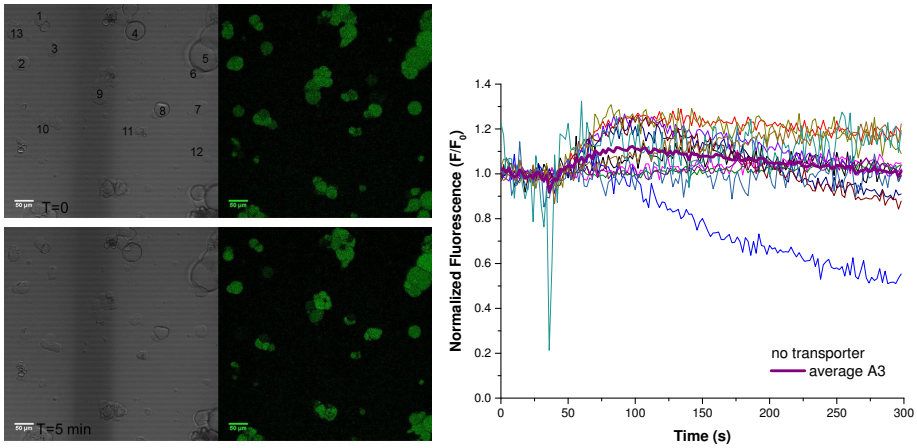

Figure A2. Bright-field and fluorescence microscopy images before (top) and after (bottom) addition of NaCl to GUVs without transporter (*experiment A3*). The normalized fluorescence intensity over time is given for the individual numbered GUVs and for the average of all numbered GUVs (fat purple line). The average diameter of the GUVs used in the average trace for 38 µm.

0.1% transporter

The decrease of fluorescence intensity before the addition of NaCl (sharp drops before t=0) in some traces is caused by the tip of the syringe used add the NaCl solution passing through the laser beam that is scanning the sample.

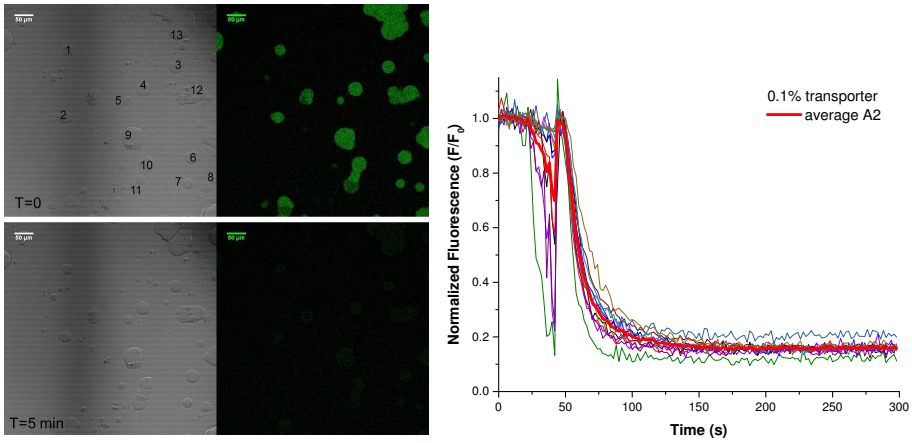

Figure A3. Bright-field and fluorescence microscopy images before (top) and after (bottom) addition of NaCl to GUVs containing 0.1% transporter (*experiment A2*). The normalized fluorescence intensity over time is given for the individual numbered GUVs and for the average of all numbered GUVs (fat red line). The average diameter of the GUVs used in the average trace for 36 µm.

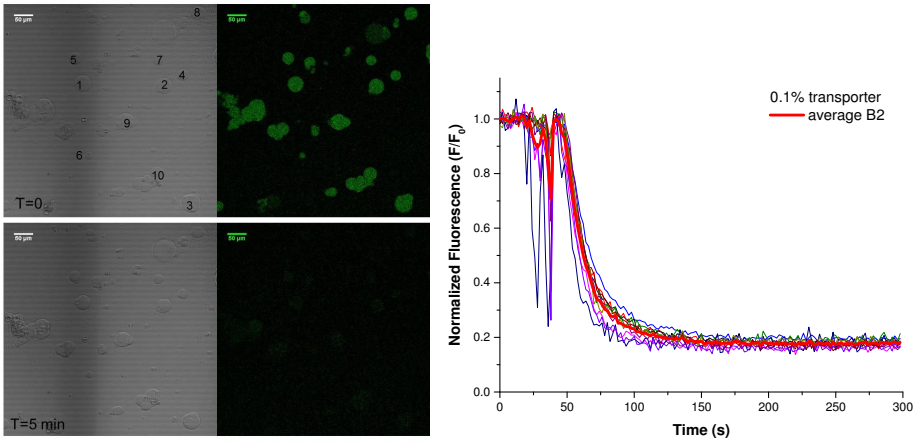

Figure A4. Bright-field and fluorescence microscopy images before (top) and after (bottom) addition of NaCl to GUVs containing 0.1% transporter (experiment B2). The normalized fluorescence intensity over time is given for the individual numbered GUVs and for the average of all numbered GUVs (fat red line). The average diameter of the GUVs used for the average trace is 36 µm.

0.04% transporter

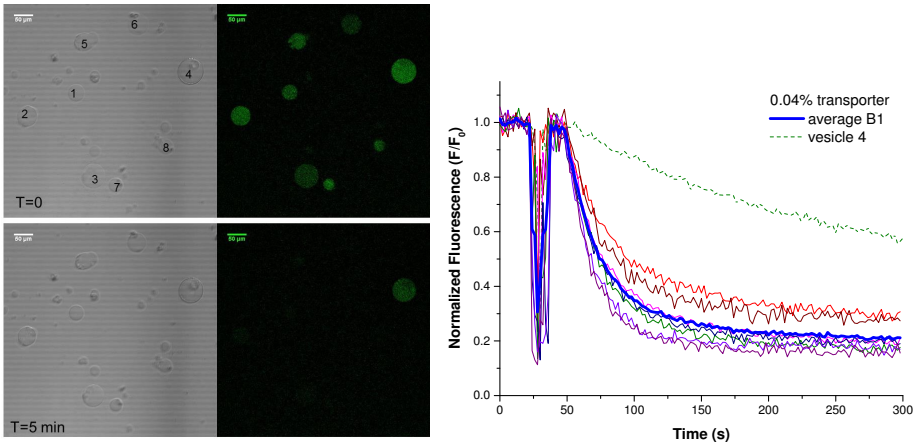

Figure A5. Bright-field and fluorescence microscopy images before (top) and after (bottom) addition of NaCl to GUVs containing 0.04% transporter (*experiment B1*). The normalized fluorescence intensity over time is given for the individual numbered GUVs and for the average of all numbered GUVs (fat blue line; excluded is vesicle 4, corresponding to green dashed line). The average diameter of the GUVs used for the average trace is 46 µm.

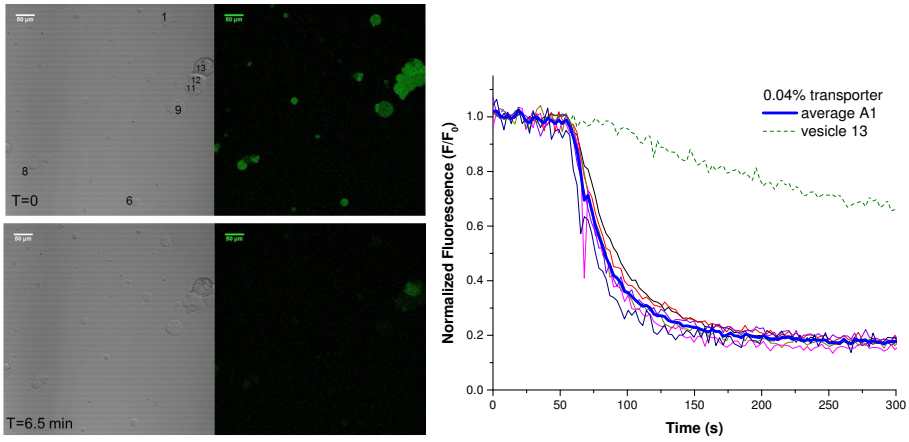

Figure A6. Bright-field and fluorescence microscopy images before (top) and after (bottom) addition of NaCl to GUVs containing 0.04% transporter (*experiment A1*). The normalized fluorescence intensity over time is given for the individual numbered GUVs and for the average of all numbered GUVs (fat blue line; excluded is vesicle 13, corresponding to green dashed line). The average diameter of the GUVs used for the average trace is 34 µm.

0.01% transporter

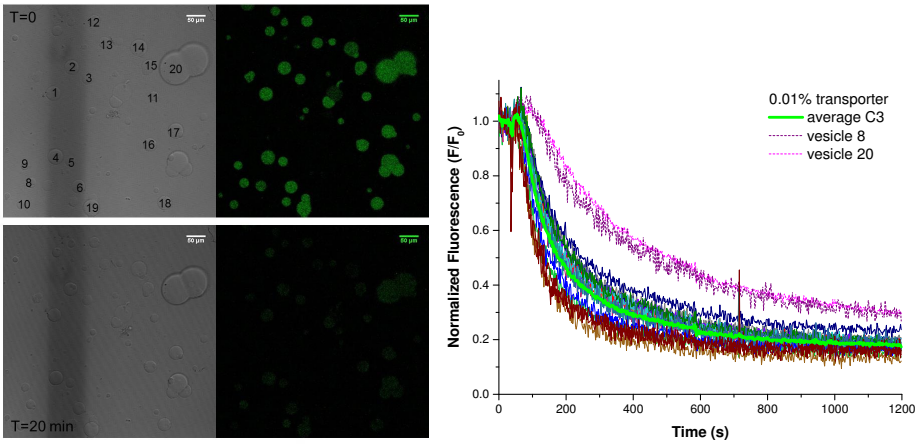

Figure A7. Bright-field and fluorescence microscopy images before (top) and after (bottom) addition of NaCl to GUVs containing 0.01% transporter (*experiment C3*). The normalized fluorescence intensity over time is given for the individual numbered GUVs and for the average of all numbered GUVs (fat light green line; excluded are vesicles 8 and 20). The average diameter of the GUVs used in the average trace for 34 µm.

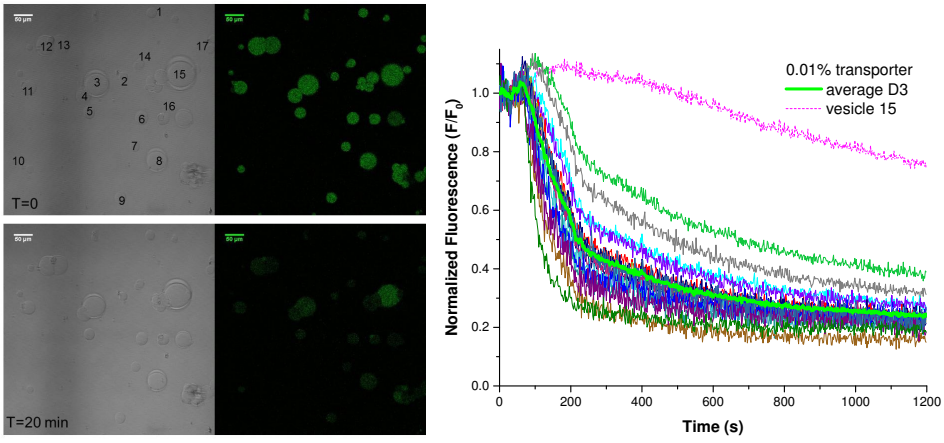

Figure A8. Bright-field and fluorescence microscopy images before (top) and after (bottom) addition of NaCl to GUVs containing 0.01% transporter (*experiment D3*). The normalized fluorescence intensity over time is given for the individual numbered GUVs and for the average of all numbered GUVs (fat light green line; excluded is vesicle 15). The average diameter of the GUVs used in the average trace for 34 µm.

0.01% transporter

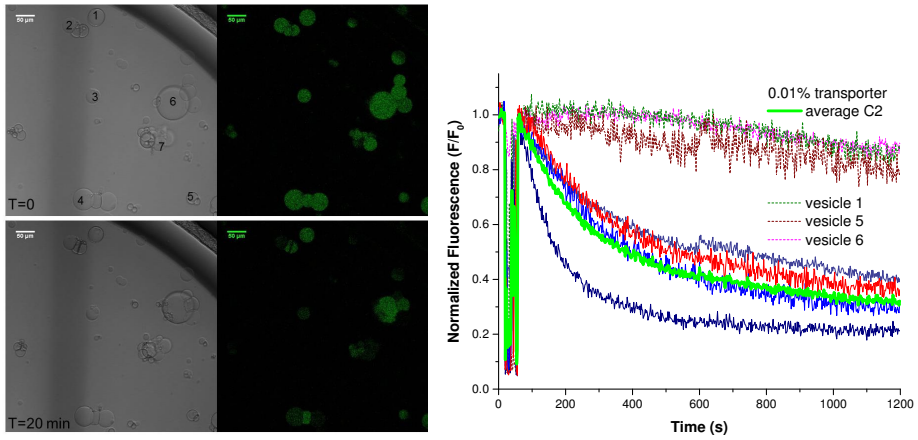

Figure A9. Bright-field and fluorescence microscopy images before (top) and after (bottom) addition of NaCl to GUVs containing 0.01% transporter (*experiment C2*). The normalized fluorescence intensity over time is given for the individual numbered GUVs and for the average of all numbered GUVs (fat light green line; excluded are vesicles 1, 5, and 6). The average diameter of the GUVs used in the average trace for 43 µm.

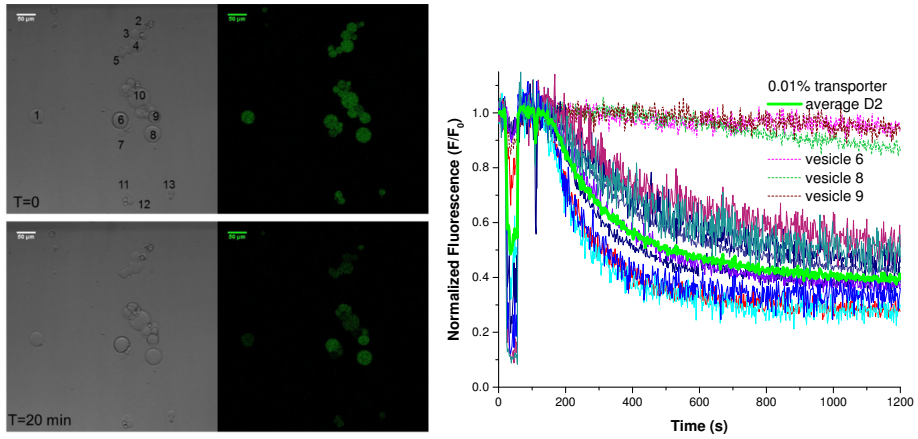

Figure A10. Bright-field and fluorescence microscopy images before (top) and after (bottom) addition of NaCl to GUVs containing 0.01% transporter (experiment D2). The normalized fluorescence intensity over time is given for the individual numbered GUVs and for the average of all numbered GUVs (fat light green line; excluded are vesicles 6, 8, and 9). The average diameter of the GUVs used in the average trace for 29 µm.

Test for photobleaching

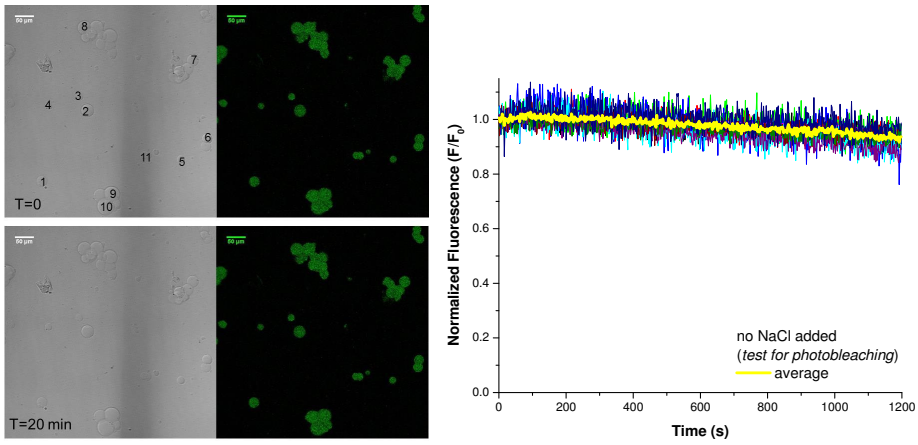

Figure A11. Bright-field and fluorescence microscopy images at the start and end of a 20 minute time lapse measurement to test for photobleaching (no NaCl added). The normalized fluorescence intensity over time is given for the individual numbered GUVs and for the average of all numbered GUVs (fat yellow line).

Cross-sections of vesicles with rhodamine-labelled membranes in Figure 4a.

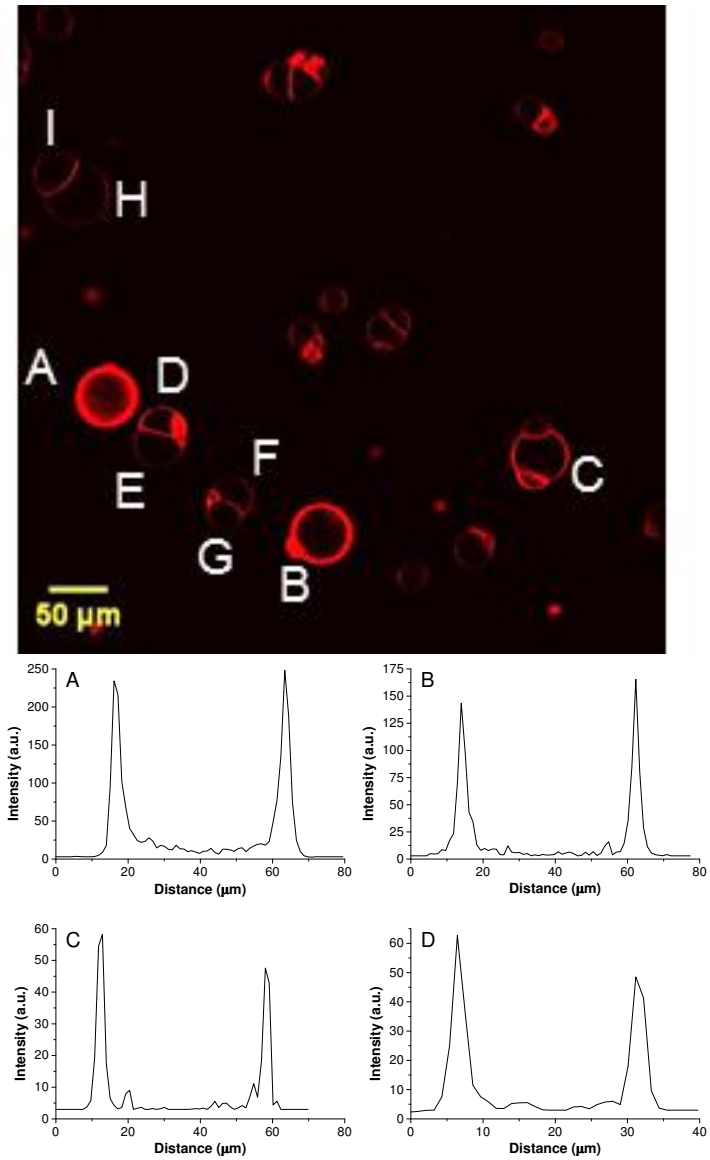

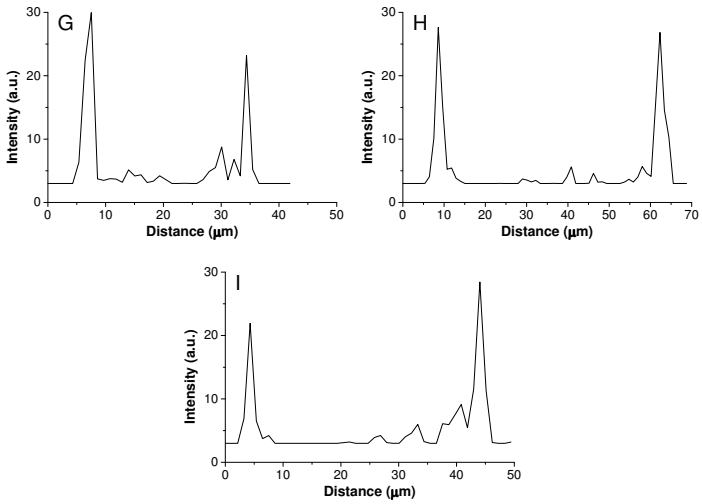

Figure A12. Fluorescence microscopy image of rhodamine labelled lipid **5** in the lipid bilayer membrane (top, copy of Figure 4a of the main paper). Intensity profiles of the cross-sections of the giant vesicles identified with a letter are given, showing intensities ~ 25 for vesicles E-G, ~ 50 for vesicles C and D, ~ 150 for B and ~ 250 for A. From the combination of these data and the transport curves in Figure 4c, we conclude that vesicles E-I are unilamellar and A-D are multilamellar.